Comparison of Methodologies in Monte Carlo for Constraining CT10 PDF Parameters Using a Novel Variable

James Hanson

Submitted under the supervision of Jeremiah Mans to the University Honors Program at the University of Minnesota-Twin Cities in partial fulfillment of the requirements for the degree of Bachelor Science, magna cum laude in Physics.

May 4, 2012

Abstract

A Monte Carlo feasibility study was performed regarding the possiblity of improving the fit values of the 26 parameters of the CT10 Parton Distribution Function using data from the Compact Muon Solenoid at the Large Hadron Collider. Two techniques, one involving direct comparison of χ^2 values ($\Delta\chi^2$) and the other involving fits of weigthed averages against data, were performed using three different measurements, including a novel variable ϕ^*, which was designed to take advantage of particle detectors good track angle resolution to circumvent their relatively poor momentum and energy resolutions. The $\Delta\chi^2$ technique failed to achieve statistically significant results for any measurement other than rapidity and the weighted average fit technique suffered from strong correlations in the effects of variations on all of the measurements considered.

1 The Compact Muon Solenoid Detector

The Large Hadron Collider (LHC) is a particle accelerator located in the Geneva region. Its primary purpose is to produce head-on 7 TeV proton-proton collisions and 2.75 TeV per nucleon ion collisions at optimal luminosities of $10^{34}\text{cm}^{-2}\text{s}^{-1}$ and $10^{27}\text{cm}^{-2}\text{cm}^{-1}$, respectively. This will be used to study the phenomenon of elctroweak symmetry breaking

The Compact Muon Solenoid (CMS) detector at the LHC is one of the two primary particle detectors at the LHC (the other being ATLAS) located at one of the two primary collision points. It consists of a 6 m diameter 12.5 m long superconducting solenoid designed to generate a 4 T magnetic field in the interior detector regions in order to enable the measurement of particle mass and charge sign. Inside the magnet the CMS detector is divided into regions. These regions are comprised of differing varieties of particle detectors, suited for the expected byproducts of the proton collisions at different positions relative to the interaction point.

The Electromagnetic Calorimeter (ECAL) is a region of the detector which consists of a series of Lead Tungstate ($PbWO_4$) crystal scintillators which produce light whenever charged particles pass through them. This light is detected by one of two varieties of photodetectors: avalanche photodiodes in the barrel and vacuum phototriodes in the endcaps.

In high energy particle physics, it is common to use a modified form of spherical coordinates where the polar angle is replaced with pseudorapidity, defined by $\eta = -\ln\left[\tan\left(\frac{\theta}{2}\right)\right]$, where θ is the polar angle.

The section of the ECAL in the pseudorapidity range $|\eta| < 1.479$ is known as the barrel (EB). It consists of a 360 by 170 grid (in ϕ and η respectively) of 230 mm (25.8 radiation lengths) long crystals. At either end of the ECAL, 315.4 cm from the interaction point, in the $1.479 < |\eta| < 3.0$ range, there are regions known as the endcaps (EE). Each consists of two halves (called Dees) consisting of 138 groups of 5x5 crystal units (supercrystals) as well as 18 special partial supercrystals at the inner and outer edges all arranged in a rectangular x-y grid. In total there are 3662 crystals in each Dee, each 220 mm (24.7 radiation lengths) long.

The Hadron Calorimeter (HCAL) is a large region of the detector intended to detect primarily hadron jets. Of primary interest to this studiy is the forward calorimeter (HF), which is 11.2 m from the interaction point and covers a pseudorapidity range of $3 < |\eta| < 5.2$. It consists of a series of quartz fibres (chosen for radiation hardness) which collect Cherenkov light from shower particles. [8]

2 The CT10 Parton Distribution Function

The predominant theory explaining the behavior of high energy proton collisions is the quark model or parton model, which posits that the proton (as well as the neutron) is composed of smaller particles known as quarks and gluons, which are held together by the strong nuclear force. The quarks and gluons in a proton come in two varieties, valence quarks, of which there are three, and virtual sea particles, which are spontaneously created and absorbed continually.

Due to the intractability of calculating proton-proton collision cross sections directly from Quantum Chromodynamics (QCD), a variety of phenomenological models have been developed. Among these are what are called parton distribution functions (PDFs). A parton distribution function is a probability density of the various partons, quarks, antiquarks, and gluons, as a function of longitudinal momentum fraction.

The PDF employed in this study, known as CT10, was developed in 2010 for analysis of LHC and Tevatron data, as a updated version of the older CTEQ6.6 (seen in figure 1). It contains 26 free

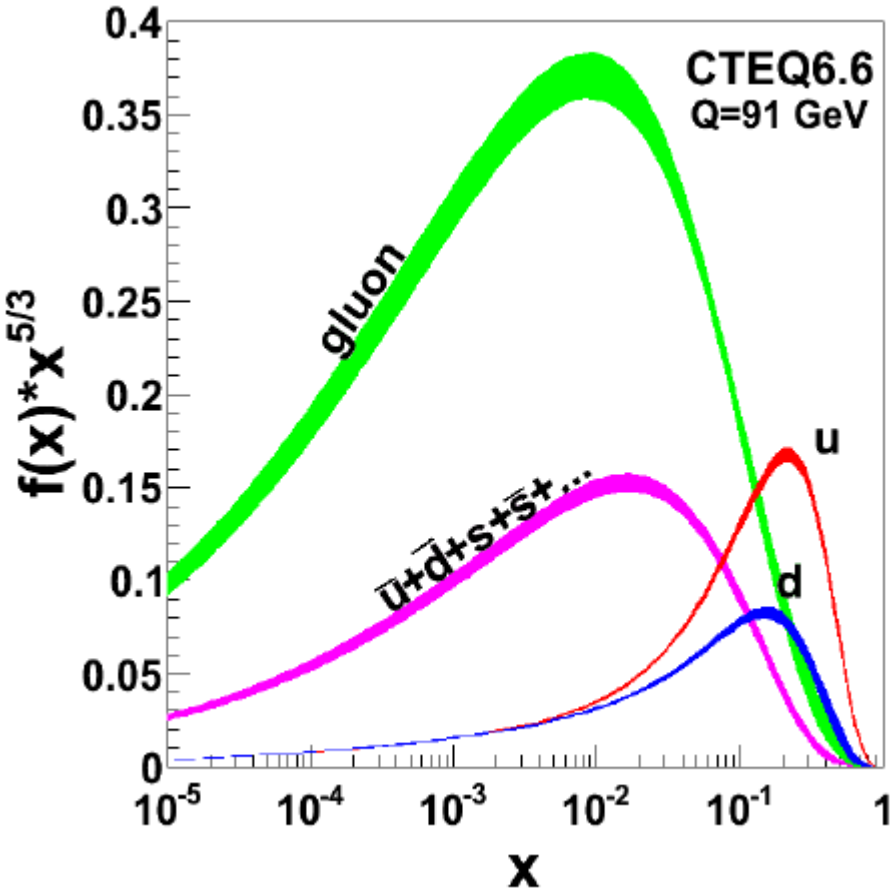

Figure 1: The CTEQ6.6 Parton Distribution Function

parameters whose values were fitted using all available data. As in any multidimensional χ^2 fit, the fit error is fully characterized by an $N \times N$ matrix, rather than a single error along each parameter, or, equivalently, as errors along the eigenvectors of this matrix in parameter space. [4]

3 Measurements of $Z \to \ell\ell$

Deep inelastic collisions between protons often produce Z bosons, which then often decay into lepton-antilepton pairs. The distribution of these Z bosons serves as a measurement of the internal properties of the proton and therefore a means of constraining PDF parameters. When two unambiguous lepton

tracks are identified they are conisdered a potential Z event.

In this study there are three categories of dilepton events of interest, classified by the detectors in whichy the final state leptons ended up, specifically events where both leptons are detected by the barrel (EB-EB), events where one is detected by the barrel and one by the endcap (EE-EB), and events where one is detected by the endcap and one the forward calorimeter (EE-HF). These categories are considered because the accuracy of energy measurements is better for leptons that end up in different parts of the detector, because of pileup effects, and the signal-to-noise ratio of HF-HF events is too poor.

3.1 Invariant Mass

The rest or invariant mass of the Z boson is equal to its energy in its frame of reference, or $\sqrt{E^2 - p^2}$ (with $c = 1$) in any frame of reference. By conservation of energy this must be equal to the total energy of the two leptons in their center of mass frame, which is a measurable quantity, still equal to $\sqrt{E^2 - p^2}$, where E and p are total energy and momentum respectively. Although the Z boson has a well-defined mass, the measured center of momentum frame energy of dileptons form broad peak with a large background for three reasons. The Z bosons produced by proton-proton collisions are virtual and can therefore be off-shell widening the peak, and dilepton final states can also be the result of a virtual photon. Also resolutions effects smear the distribution.

3.2 Rapidity

Rapidity is an alternative representation of velocity commonly used in special relativity. Defined as $\cosh^{-1} \frac{1}{\sqrt{1-v^2/c^2}}$. Its primary advantages are that the Lortentz transform has a simple form when expressed in terms of rapidity, the addition of velocities is linear in rapidity, and the rapidity of light is infinite, so rapidities can be arbitrarily large. Furthermore, it justifies the use of pseudorapidity as the distribution of rapidities of particles produced by collisions is essentially flat as a function of pseudorapidity.

Because it has a very direct relationship to momentum fractions of partons, the distribution of final state particle rapidities along the beam axis is a useful measurement for constraining PDFs. In a proton

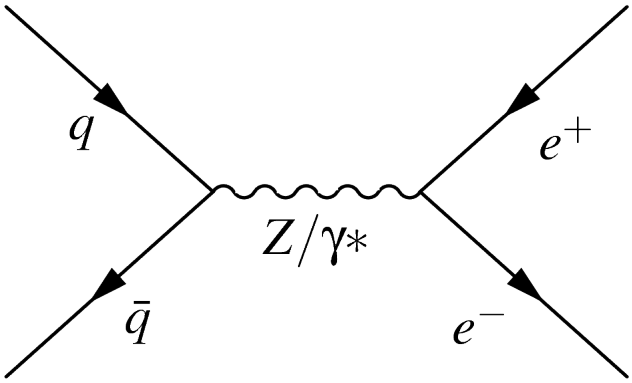

Figure 2: s-Channel Feynman Diagram

proton collision producing a Z boson from two partons (labeled 1 and 2), the energy and momentum of the Z boson are given by $E_Z = x_1\frac{\sqrt{s}}{2} + x_2\frac{\sqrt{s}}{2}$ and $p_z = x_1\frac{\sqrt{s}}{2} - x_2\frac{\sqrt{s}}{2}$, where x_1 and x_2 are the momentum fractions of partons 1 and 2 respectively and $\sqrt{s}$ is the center of mass energy of the collision. This means that the values of x_1 and x_2 are constrained by the relation $m_Z^2 = sx_1x_2$, where m_Z is the mass of the Z boson, since $E_Z^2 = p_Z^2 + m_Z^2$. The rapidity of a particle can be expressed in terms of its energy and momentum by the formula $Y_Z = \frac{1}{2}\ln\frac{E_Z+p_Z}{E_Z-p_Z}$, which reduces to $Y_Z = \frac{1}{2}\ln\frac{x_1}{x_2}$. Substituting in the constraint and reducing gives $Y_Z = \ln\frac{\sqrt{x_1}}{\sqrt{m_Z^2/sx_1}} = \ln\frac{x_1\sqrt{s}}{m_Z}$. So $x_1 = \frac{m_Z}{\sqrt{s}}e^{Y_Z}$, giving a direct relationship between momentum fraction and rapidity.

3.3 Transverse Momentum and Related Variables

The transverse momentum of a Z boson is defined as the component of its momentum perpendicular to the beam axis. This measurement is of primary interest since it distinguishes events that are results of s-channel interactions (figure 2), which result in very little transverse mometnum, and events that are the results of t-channel interactions (figure 3), which result in a broader range of transverse momentum.

The transverse momenta of the product leptons are defined analogously. These quantities are used to define two observables in terms of what is the called the thrust axis: $\hat{t} = \frac{\vec{p}_t^{(1)} - \vec{p}_t^{(2)}}{\left|\vec{p}_t^{(1)} - \vec{p}_t^{(2)}\right|}$, where $\vec{p}_t^{(1)}$ and $\vec{p}_t^{(2)}$ are the transverse momenta of the leptons. a_T and a_L are the components of the total Z transverse

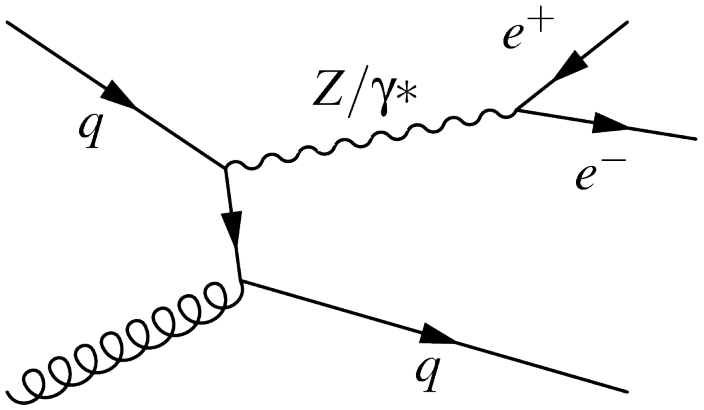

Figure 3: t-Channel Feynman Diagram

momentum, $\vec{p}_T^Z = \vec{p}_t^{(1)} - \vec{p}_t^{(2)}$ perpendicular and parallel to the thrust axis, respectively. a_T is chosen as an observable because is has been found to be less susceptible to resolution and efficency effects than p_T^Z in the $p_T^Z < 30$ GeV region [2]. In order to reduce the uncertainty in a_T measurements further it is often considered as a momentum fraction, a_T/Q, where Q is invariant dilepton mass.

3.4 Phi-Star

Due to the fact that particle detectors often have better angular resolution than momentum or energy resolution, it is advantageous to define kinematic variables which are closely correlated to desired measurements, but are entirely functions of particle track angles. A kinematic variable known as ϕ^* was recently proposed [2].

When the transverse momenta of the two leptons are approximately the same, it can be shown that $a_T/Q \approx \tan(\phi_{\text{acop}}/2)\sin(\theta^*)$, where $\phi_{\text{acop}} = \pi - \Delta\phi$, where $\Delta\phi$ is the azimuthal opening angle between the two leptons, and θ^* is the scattering angle. ϕ^* is defined accordingly as $\tan(\phi_{\text{acop}}/2)\sin(\theta^*)$ [2]. The statistical properties of this variable have been studied extensively, and it was found to be as sensitive to p_T^Z but more precisely determined given the current limitations of particle detectors [1, 2, 5].

4 Analysis

A large Monte Carlo data set was generated using the CT10 PDF in POWHEG [6, 7, 10] for boson and dilepton generation and then Pythia was used for hadronization of quarks into jets. From the full Monte Carlo data set, four independent pseudodata sets were constructed. The event populations of these pseudodata sets were chosen to be similar to the amount of data expected to be produced by CMS, specifically 4 fb^{-1} of data at 80% efficiency per lepton. This amounted to approximately 1 million events.

In order to study the ability of of these measurements to constrain the parameters of the CT10 PDF it was necessary to construct a set of datasets characterizing the effect of varying the parameters of the PDF along each eigenvector by ± 1 standard deviation. Although the variations are along eigenvalues of the fit, it should be noted that their effects on the distributions of the measurements in this study are not orthogonal.

The general analysis method used in this paper was χ^2 fitting of Monte Carlo generated mass, rapidity, and phi-star distributions with single eigenvalues of the PDF varied. "Truth" distributions, which contain the full Monte Carlo population, were varied using a weighted average parameter and fit to the psuedodata distributions. A measurement of sensitivity, $\chi^2_{i0} = \sum \frac{(d_{in}-m_{0n})^2}{\sigma^2_{in}}$, where d_{in} is the population of the nth bin of the ith variation pseudodata set (0 being no varied eigenvector) normalized by the population of the entire histogram, σ_{in} is the estimated error on d_{in}, and m_{0n} is the nth bin of the unvaried "truth" data set normalized by the population of its entire histogram, was calculated for all of the eigenvector variations for each of the measurements or pair of measurements considered and a set of six sensitive eigenvectors were selected (1, 4, 7, 10, 12, and 24 using the standard indexing scheme).

Each of the three measurements described in section 3 were considered, as well as the combination of rapidity and ϕ^*, represented by a two dimensional histogram. Neither of the other two measurements were combined with mass in the final analysis, as the sensitivity of the mass distribution to variations in the eigenvectors was found to be insignificant. The mass measurement was rebinned down to a set of six bins chosen to create consistent bin populations outside of the Z peak and the rapiditiy measurements were folded to $|Y|$ measurements, where Y is rapiditiy, in order to increase statistics, as no significant

directional asymmetry was expected. For all three measurements, the data from the three detector region pairs were combined, that is in the below formulas the bin populations are the sums of the three populations corresponding to the three detector region pairs. In the ϕ^* measurement, the uncombined values were also considered, that is the χ^2 values were taken as the sum of the χ^2 values corresponding to the three detector regions.

4.1 $\Delta\chi^2$ Method

This method consists of calculating $\tilde{X}_i = \frac{\chi^2_{i0}-\chi^2_{ii}}{\sigma\chi^2_{00}}$ for each of the variations, where $\chi^2_{ij} = \sum \frac{(d_{in}-m_{jn})^2}{\sigma^2_{in}}$ (with the values in that formula being the averages across the four pseudodata sets) and $\sigma\chi^2_{00}$ is the standard deviation of χ^2_{00} across the four pseudodata sets. $\sigma\chi^2_{00}$ represents a purely statistical significance level that would be proportional to $\sqrt{N}$, where N is the number of bins, if every bin were populated enough to be approximately normally distributed. This value represents a measurement of the statistical detectability of the effect of a 1σ variation along one of the PDF eigenvectors. If the effect is pronounced enough, $\Delta\chi^2_i = \chi^2_{i0} - \chi^2_{ii}$ should be larger than $\sigma\chi^2_{00}$, otherwise the change is indistinguishable from statistical variation.

4.2 Best Fit of Weighted Average Method

Weighted averages were used to approximate the effect of varying the PDF parameter set along each eigenvector. Each bin of the model histogram was calculated using the formula $m_i(t) = \frac{1}{2}((1+t)m_i^+ + (1-t)m_i^-)$, where t is a parameter representing a variation of up to one sigma in either direction, and $m_i^\pm$ are the normalized bin populations of the "truth" variation.

Due to the linearity of the weighted average model, the fit values and errors are analytically solvable and the derivation is below:

$$\chi^2 = \sum \frac{(d_i - m_i)^2}{\sigma_i^2}$$

$$\chi^2 = \sum \frac{((1+t)m_i^+ + (1-t)m_i^- - 2d_i)^2}{4\sigma_i^2}$$

$$\chi^2 = \sum \frac{((m_i^+ - m_i^-)t + m_i^+ + m_i^- - 2d_i)^2}{4\sigma_i^2}$$

$$\chi^2 = \sum \frac{(m_i^+ - m_i^-)^2 t^2 - 2(m_i^+ - m_i^-)(m_i^+ + m_i^- - 2d_i)t + (m_i^+ + m_i^- - 2d_i)^2}{4\sigma_i^2}$$

$$\chi^2 = t^2 \sum \frac{(m_i^+ - m_i^-)^2}{4\sigma_i^2} - t \sum \frac{2(m_i^+ - m_i^-)(m_i^+ + m_i^- - 2d_i)}{4\sigma_i^2} + \sum \frac{(m_i^+ + m_i^- - 2d_i)^2}{4\sigma_i^2}$$

A parabola in the form $at^2 + bt + c$ can be written $c - \frac{b^2}{4a} + a\left(t + \frac{b}{2a}\right)^2$, and is therefore minimized (or maximized) by $t = -\frac{b}{2a}$. This gives the formulas for t_{min}, σ_t, and χ^2_{min}:

$$t_{min} = \sigma_t^2 \sum \frac{(m_i^+ - m_i^-)(m_i^+ + m_i^- - 2d_i)}{4\sigma_i^2}$$

$$\sigma_t = \left[\sum \frac{(m_i^+ - m_i^-)^2}{4\sigma_i^2}\right]^{-1/2}$$

$$\chi^2_{min} = \sum \frac{(m_i^+ + m_i^- - 2d_i)^2}{4\sigma_i^2} - \sigma_t^2 \left[\sum \frac{(m_i^+ - m_i^-)(m_i^+ + m_i^- - 2d_i)}{4\sigma_i^2}\right]^2$$

By fitting pseudodata variations against weighted average models for each pair of sensitive eigenvectors it can be determined how well this method delineates the effects of variations in each eigenvector. Ideally the fit parameter t should only significantly deviate from 0 when the eigenvector is being fitted against itself. The final fit values were taken as the average across the four pseudodata sets and the fit errors were taken to be the standard deviation of them. These values were checked for consistency with the error estimated by the formula above.

In order to evaluate the degree to which variations in eigenvectors were correlated, a quantity representing correlation was calculated: $\sum_d \frac{t_{di} t_{dj}}{\sigma_{di} \sigma_{dj}}$, where t_{dk} is the best fit of the pseudodata represented by the index d (which includes eigenvector index, plus or minus variation, and pseudodata set for a total of $26 \times 2 \times 4 = 208$ terms in the sum) against the model which is varied along the eigenvector k. Then

for each measurement, the histogram of this value for all pairs $i \neq j$ (without duplicates, making 325 pairs) was fitted by a multiple gaussian. Any well-defined peaks away from zero were an indication of a set of correlated eigenvectors.

5 Results

The full results are included in the appendix. With the $\Delta\chi^2$ method, the mass measurement was very insensitive to eigenvector variations, with the largest ratio being $\tilde{X}_{10-} = 0.40$, with $\sigma\chi^2_{00} = 3.85$. For the rapidity measurement, the values were somewhat better, with most values near 1, although several below 0.5, with $\sigma\chi^2_{00} = 22.42$. For the ϕ^* measurement with combined detector region pairs, $\sigma\chi^2_{00}$ wasn't significantly larger, at 32.39, but the values of $\Delta\chi^2_i$ were significantly smaller, with a maximum value of $\tilde{X}_{4+} = 0.18$ and several negative values, a strong indication of statistical effects dominating. For the ϕ^* measurement with separated detector region pairs, $\sigma\chi^2_{00} = 82.60$. The values of $\Delta\chi^2_i$ were significantly larger, comparable to the mass values, with a maximum of $\tilde{X}_{4+} = 0.40$, the same eigenvector and direction as the combined measurement. For the two dimensional ϕ^* rapidity measurement, $\sigma\chi^2_{00} = 1067.26$. The $\Delta\chi^2_i$ values were comparably small, with a maximum of $\tilde{X}_{7+} = 0.08$ and a couple negative values.

With the weighted average fit method, the mass measurement resulted in large fit errors, usually on the order of 1, except for fits against the 10th eigenvector "truth" model, which had fit errors of approximately 0.23-0.24. For the rapidity measurement, the fit errors were typically closer to 0.25, but many of the fits for distinct eigenvectors were more than 1σ away from 0 or less than 1σ away from ± 1. For the combined ϕ^* measurement, the fit errors were larger than one for al lbut the fits against the 4th eigenvector, and were even as large as 2 and 4 for fits against the 12th and 24th eigenvectors respectively. For the separated ϕ^* measurement, the fit errors were significantly smaller, always less than 0.42. However the fit values were often several σ away from 0 for distinct eigenvector fits. For the two dimensional ϕ^* rapidity measurement, the fit errors were always less than 0.38, however many of the fit values were several σ away from 0 for distinct eigenvector fits.

The results of the correlation analysis are given in figures 4-8 in the appendix. Each histogram is

fitted with the sum of 2, 3, or 5 gaussians, depending on the distribution seen in the histogram. All of the measurements except mass and the separated ϕ^* are fit well with the sum of 3 gaussians. Mass is fit with the sum of 2 and the separated ϕ^* measurement is fit with the sum of 5. In all of the measurements except mass and the two dimensional ϕ^* v Rapidity measurement there are large peaks that are far from zero, indicating sets of correlated eigenvectors. Although there seem to be two peaks in the mass case, they overlap significantly and the two off-zero peaks in the two dimensional measurement are smaller than the central peak.

6 Conclusions

Of the measurements studied, in the $\Delta\chi^2$ method, only the one dimensional rapidity measurement was able to create statistically significant differences between the variation and the base. Low and negative values of $\tilde{X}_i$ indicate that statistical effects dominate the one and two dimensional ϕ^* measurements.

For the weighted average model method, the results indicated an inability to delineate the effects of variations in each eigenvector as every pseudodata variation resulted in significant variations in the fits in models where other eigenvectors were being varied. This is verified by the correlation analysis which shows large off-zero peaks in all of the measurements except mass.

7 Future Research

Obvious avenues for further research are investigating a larger set of CT10's eigenvectors, other PDFs, and other measurement variables. Furthermore, techniques to compensate for the correlations in the effects on the measured variables with variations along the eigenvectors might be investigated.

8 References

[1] A. Banfi, M. Dasgupta, S. Marzani, and L. Tomlinson. JHEP 01 (2012) 044, arXiv:1110.4009v2.

[2] A. Banfi, S. Redford, M. Vesterinen, P. Waller, and T. R. Wyatt. Eur. Phys. J. C 71, 1600 (2011),

arXiv:1009.1580v2.

[3] DØ Collaboration. DØ Note 5755-CONF (2008).

[4] H. Lai, M. Guzzi, J. Huston, Z. Li, P. M. Nadolsky, J. Pumplin, and C.-P. Yuan. Phys. Rev. D 82, 074024, (2010), arXiv:1007.2241v3.

[5] M. Vesterinen and T.R. Wyatt. Nucl. Instrum. Meth. A 602, 432-437 (2009), arXiv:0807.4956v1.

[6] P. Nason, JHEP 0411 (2004) 040, hep-ph/0409146

[7] S. Alioli, P. Nason, C. Oleari and E. Re, JHEP 1006 (2010) 043, arXiv:1002.2581.

[8] S. Chatrchyan et al. (CMS), JINST 3, S08004 (2008).

[9] S. Chatrchyan et al. (CMS), Phys. Rev. D 85, 032002 (20).

[10] S. Frixione, P. Nason and C. Oleari, JHEP 0711 (2007) 070, arXiv:0709.2092.

9 Appendix: Tables of Values and Correlation Histograms

Table 1: $\Delta\chi_i^2$ of Mass Measurement

Index (Variation)	$\Delta\chi_i^2$	$\sigma\chi_{00}^2$	$\Delta\chi_i^2/\sigma\chi_{00}^2$
1+	0.6914	3.8453	0.1798
1-	0.1433	3.8453	0.0373
4+	0.8044	3.8453	0.2092
4-	0.5773	3.8453	0.1501
7+	1.4654	3.8453	0.3811
7-	-0.1596	3.8453	-0.0415
10+	0.2902	3.8453	0.0755
10-	1.5225	3.8453	0.3959
12+	-0.1583	3.8453	-0.0412
12-	0.9198	3.8453	0.2392
24+	-0.0406	3.8453	-0.0106
24-	0.4095	3.8453	0.1065

Table 2: $\Delta\chi_i^2$ of Rapidity Measurement

Index (Variation)	$\Delta\chi_i^2$	$\sigma\chi_{00}^2$	$\Delta\chi_i^2/\sigma\chi_{00}^2$
1+	15.2628	22.4219	0.6807
1-	19.0180	22.4219	0.8482
4+	45.3682	22.4219	2.0234
4-	30.4534	22.4219	1.3582
7+	38.6475	22.4219	1.7236
7-	14.5241	22.4219	0.6478
10+	3.7307	22.4219	0.1664
10-	22.0912	22.4219	0.9853
12+	13.6696	22.4219	0.6097
12-	29.6501	22.4219	1.3224
24+	14.3943	22.4219	0.6420
24-	18.6846	22.4219	0.8333

Table 3: $\Delta\chi_i^2$ of Combined ϕ^* Measurement

Index (Variation)	$\Delta\chi_i^2$	$\sigma\chi_{00}^2$	$\Delta\chi_i^2/\sigma\chi_{00}^2$
1+	1.3246	32.3911	0.0409
1-	-0.3644	32.3911	-0.0113
4+	5.7286	32.3911	0.1769
4-	1.5668	32.3911	0.0484
7+	1.6106	32.3911	0.0497
7-	-0.4361	32.3911	-0.0135
10+	-0.0014	32.3911	-0.00004
10-	0.4923	32.3911	0.0152
12+	-0.0867	32.3911	-0.0027
12-	-0.1093	32.3911	-0.0034
24+	-0.3683	32.3911	-0.0114
24-	-0.2034	32.3911	-0.0063

Table 4: $\Delta\chi_i^2$ of Separated ϕ^* Measurement

Index (Variation)	$\Delta\chi_i^2$	$\sigma\chi_{00}^2$	$\Delta\chi_i^2/\sigma\chi_{00}^2$
1+	16.3878	82.5998	0.1984
1-	10.9097	82.5998	0.1321
4+	33.1705	82.5998	0.4016
4-	24.2428	82.5998	0.2935
7+	32.8993	82.5998	0.3983
7-	6.9426	82.5998	0.0841
10+	1.8856	82.5998	0.0228
10-	19.5482	82.5998	0.2367
12+	4.3869	82.5998	0.0531
12-	23.4310	82.5998	0.2837
24+	3.6117	82.5998	0.0437
24-	13.6708	82.5998	0.1655

Table 5: $\Delta\chi_i^2$ of ϕ^* v Rapidity Measurement

Index (Variation)	$\Delta\chi_i^2$	$\sigma\chi_{00}^2$	$\Delta\chi_i^2/\sigma\chi_{00}^2$
1+	50.6408	1067.2600	0.0474
1-	-23.4226	1067.2600	-0.0219
4+	37.9835	1067.2600	0.0356
4-	21.4985	1067.2600	0.0201
7+	81.6129	1067.2600	0.0765
7-	-16.9441	1067.2600	-0.0159
10+	-6.5945	1067.2600	-0.0062
10-	47.0931	1067.2600	0.0441
12+	-22.1549	1067.2600	-0.0208
12-	50.7373	1067.2600	0.0475
24+	-26.8651	1067.2600	-0.0252
24-	29.6617	1067.2600	0.0278

Table 6: Mass Fit Values

D	T	t_{min}	σ_t	D	T	t_{min}	σ_t	D	T	t_{min}	σ_t	D	T	t_{min}	σ_t
0	1	0.39	0.80												
0	4	-0.04	0.85												
0	7	0.26	0.68												
0	10	0.55	0.24												
0	12	-0.50	0.81												
0	24	-0.79	0.97												
1+	**1**	**1.33**	**0.81**	1+	10	0.00	0.24	4+	1	-0.65	0.82	4+	10	1.31	0.24
1-	**1**	**-0.63**	**0.79**	1-	10	1.14	0.24	4-	1	1.30	0.78	4-	10	-0.13	0.23
1+	4	-0.60	0.86	1+	12	-1.45	0.83	**4+**	**4**	**1.01**	**0.86**	4+	12	0.37	0.83
1-	4	0.58	0.84	1-	12	0.54	0.80	**4-**	**4**	**-1.00**	**0.84**	4-	12	-1.23	0.80
1+	7	1.14	0.69	1+	24	-1.99	0.99	4+	7	-0.51	0.69	4+	24	0.34	0.99
1-	7	-0.69	0.67	1-	24	0.51	0.96	4-	7	0.91	0.67	4-	24	-1.75	0.96
7+	1	1.70	0.78	7+	10	-0.15	0.25	10+	1	-0.15	0.80	**10+**	**10**	**1.09**	**0.24**
7-	1	-0.30	0.81	7-	10	0.89	0.23	10-	1	1.90	0.78	**10-**	**10**	**-0.95**	**0.23**
7+	4	-0.70	0.84	7+	12	-1.88	0.81	10+	4	0.37	0.86	10+	12	-0.02	0.82
7-	4	0.25	0.86	7-	12	0.27	0.82	10-	4	-1.19	0.84	10-	12	-1.82	0.80
7+	7	**1.54**	**0.68**	7+	24	-2.52	0.96	10+	7	-0.19	0.69	10+	24	-0.14	0.98
7-	7	**-0.45**	**0.69**	7-	24	0.16	0.98	10-	7	1.50	0.67	10-	24	-2.59	0.96
12+	1	-0.40	0.83	12+	10	0.87	0.19	24+	1	-0.45	0.73	24+	10	0.94	0.17
12-	1	1.48	0.78	12-	10	-0.08	0.28	24-	1	1.10	0.82	24-	10	0.06	0.26
12+	4	0.20	0.90	**12+**	**12**	**0.44**	**0.82**	24+	4	0.17	0.84	24+	12	0.49	0.73
12-	4	-0.73	0.81	**12-**	**12**	**-1.58**	**0.80**	24-	4	-0.57	0.85	24-	12	-1.16	0.84
12+	7	-0.61	0.69	12+	24	0.35	0.98	24+	7	-0.67	0.59	**24+**	**24**	**0.43**	**0.86**
12-	7	1.26	0.68	12-	24	-2.15	0.96	24-	7	0.87	0.71	**24-**	**24**	**-1.64**	**1.01**

Table 7: Rapidity Fit Values

D	T	t_{min}	σ_t	D	T	t_{min}	σ_t	D	T	t_{min}	σ_t	D	T	t_{min}	σ_t
0	1	0.03	0.29												
0	4	0.00	0.18												
0	7	-0.43	0.21												
0	10	0.55	0.33												
0	12	0.37	0.18												
0	24	0.37	0.28												
1+	**1**	**0.98**	**0.29**	1+	10	-0.60	0.33	4+	1	-1.43	0.30	4+	10	2.49	0.34
1-	**1**	**-1.02**	**0.30**	1-	10	1.81	0.33	4-	1	1.34	0.29	4-	10	-1.21	0.32
1+	4	-0.60	0.18	1+	12	-0.34	0.18	**4+**	**4**	**1.05**	**0.18**	4+	12	1.71	0.18
1-	4	0.66	0.18	1-	12	1.13	0.18	**4-**	**4**	**-0.95**	**0.17**	4-	12	-0.87	0.18
1+	7	0.25	0.21	1+	24	-0.45	0.28	4+	7	-1.68	0.22	4+	24	1.88	0.29
1-	7	-1.16	0.21	1-	24	1.25	0.28	4-	7	0.73	0.21	4-	24	-1.03	0.28
7+	1	1.40	0.29	7+	10	-1.37	0.33	10+	1	-0.38	0.29	**10+**	**10**	**1.07**	**0.33**
7-	1	-0.67	0.29	7-	10	1.53	0.33	10-	1	1.17	0.29	**10-**	**10**	**-0.93**	**0.34**
7+	4	-1.06	0.18	7+	12	-1.06	0.19	10+	4	0.28	0.17	10+	12	0.71	0.18
7-	4	0.54	0.18	7-	12	1.09	0.18	10-	4	-0.80	0.18	10-	12	-0.65	0.20
7+	**7**	**0.90**	**0.22**	7+	24	-1.26	0.29	10+	7	-0.75	0.21	10+	24	0.76	0.28
7-	**7**	**-1.10**	**0.21**	7-	24	1.20	0.28	10-	7	0.52	0.22	10-	24	-0.78	0.30
12+	1	-0.61	0.28	12+	10	1.48	0.32	24+	1	-0.71	0.27	24+	10	1.50	0.30
12-	1	1.20	0.30	12-	10	-1.12	0.34	24-	1	0.90	0.30	24-	10	-0.78	0.33
12+	4	0.52	0.17	**12+**	**12**	**1.08**	**0.17**	24+	4	0.51	0.16	24+	12	1.00	0.16
12-	4	-0.92	0.18	**12-**	**12**	**-0.90**	**0.19**	24-	4	-0.74	0.18	24-	12	-0.68	0.19
12+	7	-1.07	0.20	12+	24	1.15	0.27	24+	7	-1.05	0.19	**24+**	**24**	**1.15**	**0.25**
12-	7	0.73	0.22	12-	24	-1.03	0.29	24-	7	0.55	0.22	**24-**	**24**	**-0.85**	**0.29**

Table 8: Combined ϕ^* Fit Values

D	T	t_{min}	σ_t	D	T	t_{min}	σ_t	D	T	t_{min}	σ_t	D	T	t_{min}	σ_t
0	1	0.90	1.50												
0	4	0.36	0.55												
0	7	0.88	1.25												
0	10	0.19	2.20												
0	12	1.18	2.64												
0	24	-0.27	4.12												
1+	**1**	**1.85**	**1.50**	1+	10	0.30	2.19	4+	1	3.49	1.48	4+	10	0.42	2.20
1-	**1**	**-0.14**	**1.50**	1-	10	0.08	2.20	4-	1	-1.89	1.52	4-	10	-0.02	2.19
1+	4	0.71	0.55	1+	12	2.34	2.64	**4+**	**4**	**1.33**	0.54	4+	12	4.34	2.62
1-	4	-0.03	0.55	1-	12	-0.09	2.65	**4-**	**4**	**-0.69**	0.56	4-	12	-2.20	2.66
1+	7	1.79	1.25	1+	24	0.63	4.10	4+	7	3.36	1.23	4+	24	2.11	4.13
1-	7	-0.11	1.24	1-	24	-1.25	4.14	4-	7	-1.81	1.27	4-	24	-2.78	4.11
7+	1	1.88	1.51	7+	10	-0.37	2.20	10+	1	0.94	1.49	**10+**	**10**	**0.74**	**2.13**
7-	1	0.02	1.49	7-	10	0.51	2.19	10-	1	0.83	1.51	**10-**	**10**	**-1.30**	**2.38**
7+	4	0.72	0.55	7+	12	2.00	2.67	10+	4	0.37	0.55	10+	12	1.49	2.62
7-	4	0.03	0.55	7-	12	0.32	2.63	10-	4	0.33	0.55	10-	12	0.39	2.71
7+	**7**	**1.95**	**1.26**	7+	24	-0.44	4.16	10+	7	0.83	1.25	10+	24	0.54	4.05
7-	**7**	**-0.05**	**1.24**	7-	24	-0.45	4.09	10-	7	1.07	1.26	10-	24	-2.42	4.32
12+	1	0.93	1.49	12+	10	0.85	2.16	24+	1	0.52	1.52	24+	10	0.78	2.23
12-	1	-0.09	1.51	12-	10	-0.51	2.23	24-	1	0.34	1.50	24-	10	-0.28	2.20
12+	4	0.37	0.54	**12+**	**12**	**1.60**	**2.59**	24+	4	0.21	0.56	24+	12	1.03	2.67
12-	4	-0.02	0.55	**12-**	**12**	**-0.39**	**2.68**	24-	4	0.15	0.55	24-	12	0.26	2.65
12+	7	0.78	1.25	12+	24	0.83	3.99	24+	7	0.39	1.28	**24+**	**24**	**0.43**	**4.12**
12-	7	0.06	1.26	12-	24	-2.18	4.23	24-	7	0.42	1.25	**24-**	**24**	**-1.46**	**4.14**

Table 9: Separated ϕ^* Fit Values

D	T	t_{min}	σ_t	D	T	t_{min}	σ_t	D	T	t_{min}	σ_t	D	T	t_{min}	σ_t
0	1	0.18	0.35												
0	4	0.00	0.17												
0	7	-0.28	0.29												
0	10	0.44	0.40												
0	12	0.20	0.32												
0	24	0.14	0.35												
1+	**1**	**1.14**	**0.34**	1+	10	-0.72	0.40	4+	1	-1.05	0.35	4+	10	2.22	0.41
1-	**1**	**-0.86**	**0.35**	1-	10	1.71	0.40	4-	1	1.27	0.34	4-	10	-1.16	0.40
1+	4	-0.54	0.16	1+	12	-0.60	0.32	**4+**	**4**	**1.04**	**0.17**	4+	12	1.61	0.32
1-	4	0.58	0.17	1-	12	1.07	0.32	**4-**	**4**	**-0.97**	**0.16**	4-	12	-1.09	0.32
1+	7	0.49	0.29	1+	24	-0.81	0.35	4+	7	-1.41	0.29	4+	24	1.75	0.35
1-	7	-1.11	0.29	1-	24	1.16	0.35	4-	7	0.74	0.29	4-	24	-1.33	0.35
7+	1	1.53	0.34	7+	10	-1.39	0.40	10+	1	-0.20	0.34	**10+**	**10**	**0.96**	**0.40**
7-	1	-0.52	0.34	7-	10	1.38	0.40	10-	1	1.27	0.35	**10-**	**10**	**-1.04**	**0.42**
7+	4	-0.90	0.17	7+	12	-1.20	0.32	10+	4	0.25	0.16	10+	12	0.58	0.31
7-	4	0.43	0.16	7-	12	0.91	0.32	10-	4	-0.74	0.18	10-	12	-0.87	0.34
7+	**7**	**1.04**	0.29	7+	24	-1.57	0.35	10+	7	-0.62	0.28	10+	24	0.58	0.34
7-	**7**	**-0.96**	0.29	7-	24	1.01	0.35	10-	7	0.70	0.31	10-	24	-1.13	0.37
12+	1	-0.43	0.34	12+	10	1.28	0.39	24+	1	-0.48	0.33	24+	10	1.31	0.38
12-	1	1.26	0.35	12-	10	-1.10	0.41	24-	1	0.96	0.35	24-	10	-0.74	0.41
12+	4	0.45	0.16	**12+**	**12**	**0.93**	**0.31**	24+	4	0.43	0.14	24+	12	0.89	0.29
12-	4	-0.86	0.17	**12-**	**12**	**-1.06**	**0.33**	24-	4	-0.65	0.17	24-	12	-0.78	0.32
12+	7	-0.87	0.28	12+	24	0.96	0.34	24+	7	-0.88	0.27	**24+**	**24**	**0.94**	**0.32**
12-	7	0.78	0.29	12-	24	-1.33	0.36	24-	7	0.58	0.29	**24-**	**24**	**-1.05**	**0.35**

Table 10: ϕ^* v Rapidity Fit Values

D	T	t_{min}	σ_t	D	T	t_{min}	σ_t	D	T	t_{min}	σ_t	D	T	t_{min}	σ_t
0	1	1.32	0.25												
0	4	0.05	0.15												
0	7	0.47	0.24												
0	10	-0.42	0.31												
0	12	-0.50	0.23												
0	24	-0.59	0.36												
1+	**1**	**2.26**	**0.25**	1+	10	-1.50	0.31	4+	1	0.10	0.25	4+	10	1.30	0.32
1-	**1**	**0.28**	**0.25**	1-	10	0.75	0.31	4-	1	2.39	0.25	4-	10	-1.97	0.31
1+	4	-0.47	0.15	1+	12	-1.17	0.23	**4+**	**4**	**1.09**	**0.15**	4+	12	0.78	0.23
1-	4	0.61	0.15	1-	12	0.23	0.24	**4-**	**4**	**-0.91**	**0.15**	4-	12	-1.68	0.24
1+	7	1.15	0.24	1+	24	-1.37	0.35	4+	7	-0.60	0.24	4+	24	0.79	0.38
1-	7	-0.25	0.24	1-	24	0.25	0.37	4-	7	1.45	0.24	4-	24	-1.86	0.35
7+	1	2.65	0.25	7+	10	-2.26	0.32	10+	1	0.94	0.25	**10+**	**10**	**0.09**	**0.31**
7-	1	0.62	0.25	7-	10	0.52	0.31	10-	1	2.39	0.25	**10-**	**10**	**-1.89**	**0.32**
7+	4	-0.89	0.15	7+	12	-1.85	0.23	10+	4	0.31	0.15	10+	12	-0.17	0.23
7-	4	0.51	0.15	7-	12	0.18	0.23	10-	4	-0.68	0.15	10-	12	-1.47	0.25
7+	**7**	**1.78**	0.24	7+	24	-2.15	0.35	10+	7	0.16	0.24	10+	24	-0.21	0.36
7-	**7**	**-0.20**	0.24	7-	24	0.20	0.37	10-	7	1.39	0.25	10-	24	-1.69	0.36
12+	1	0.75	0.24	12+	10	0.40	0.30	24+	1	0.66	0.23	24+	10	0.42	0.28
12-	1	2.35	0.25	12-	10	-1.95	0.32	24-	1	2.10	0.25	24-	10	-1.67	0.32
12+	4	0.52	0.14	**12+**	**12**	**0.21**	**0.23**	24+	4	0.48	0.13	24+	12	0.10	0.21
12-	4	-0.83	0.15	**12-**	**12**	**-1.73**	**0.23**	24-	4	-0.65	0.15	24-	12	-1.50	0.24
12+	7	-0.11	0.24	12+	24	0.14	0.37	24+	7	-0.09	0.23	**24+**	**24**	**0.13**	**0.36**
12-	7	1.52	0.24	12-	24	-1.90	0.35	24-	7	1.38	0.24	**24-**	**24**	**-1.74**	**0.35**

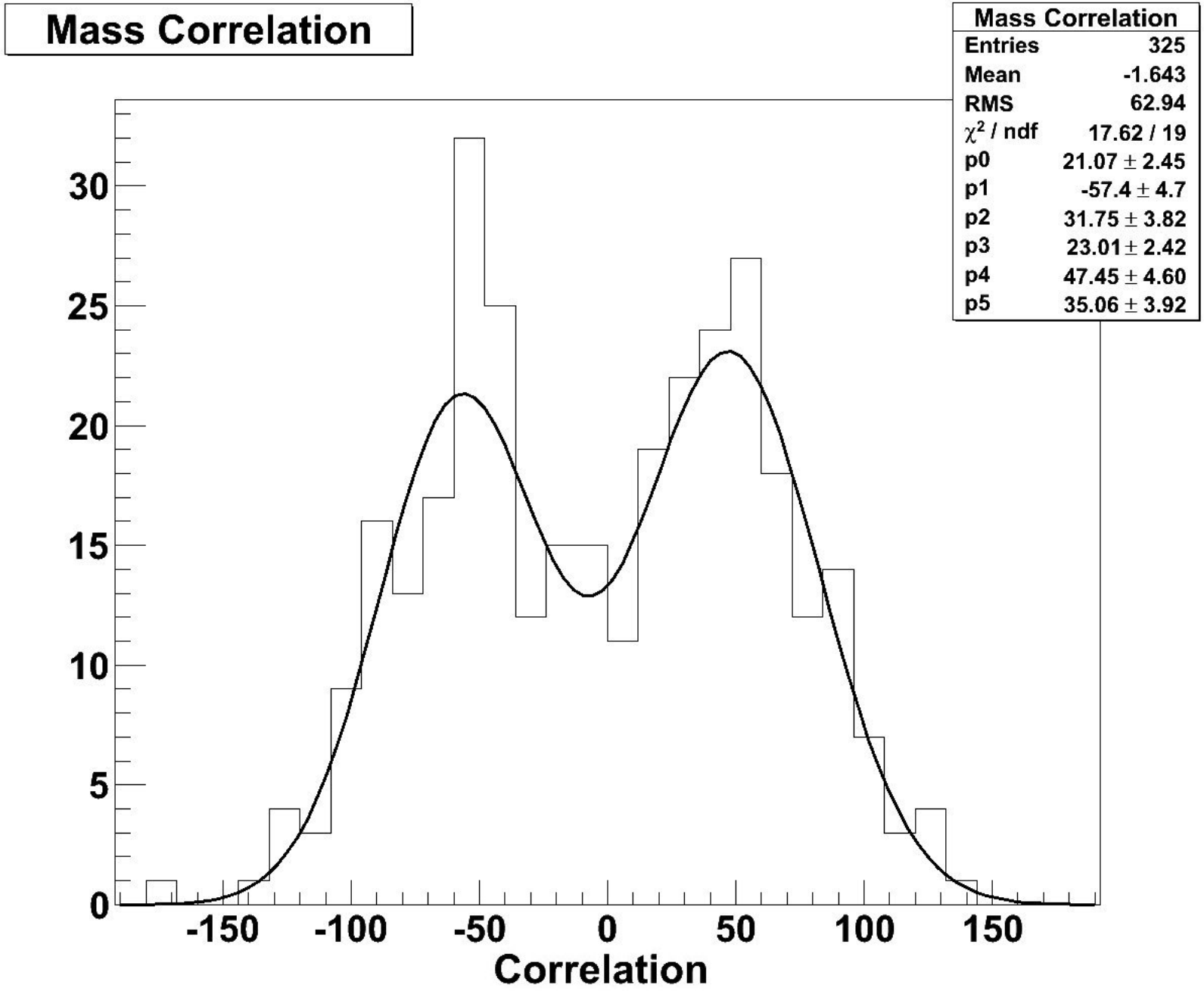

Figure 4: Mass Correlation

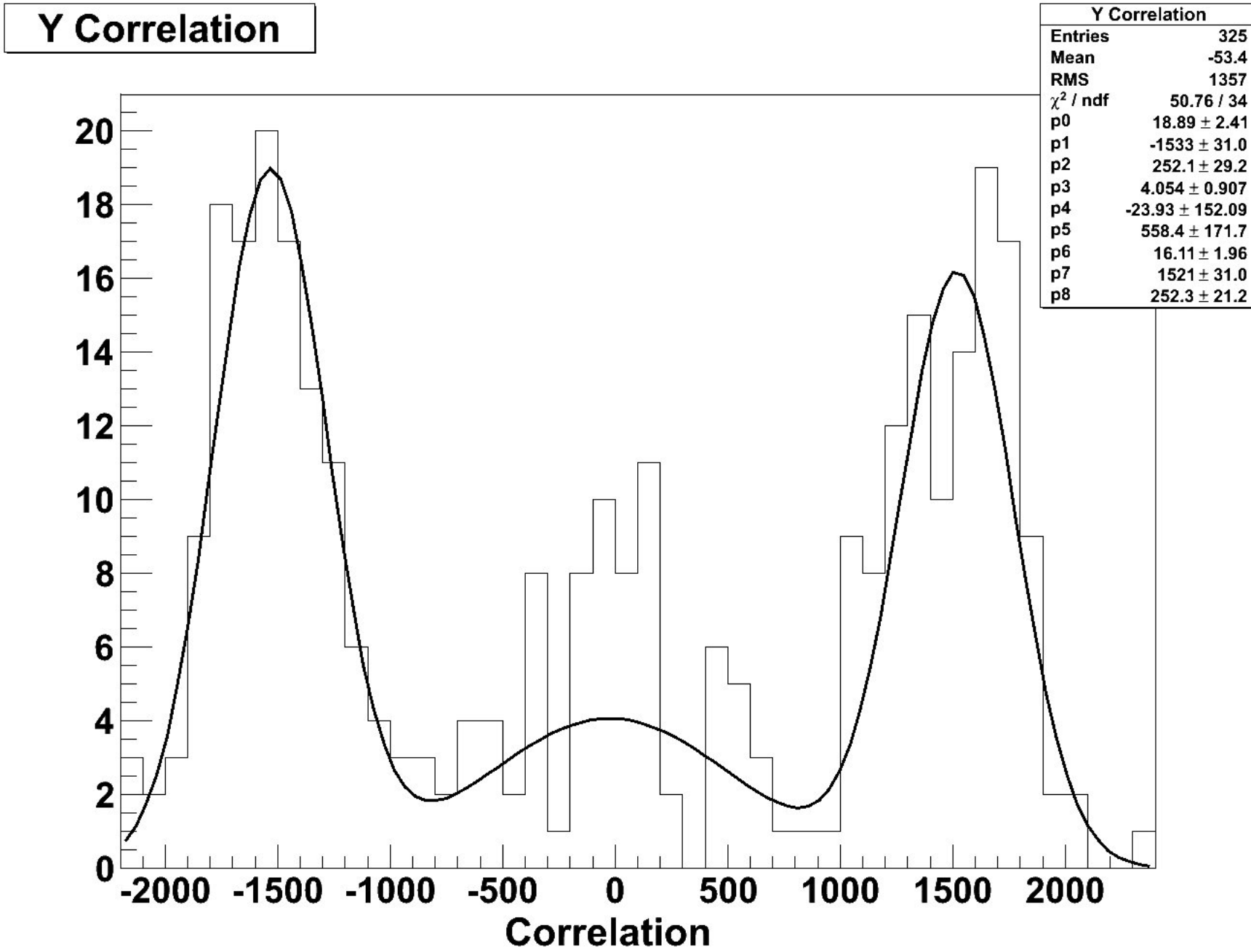

Figure 5: Rapidity Correlation

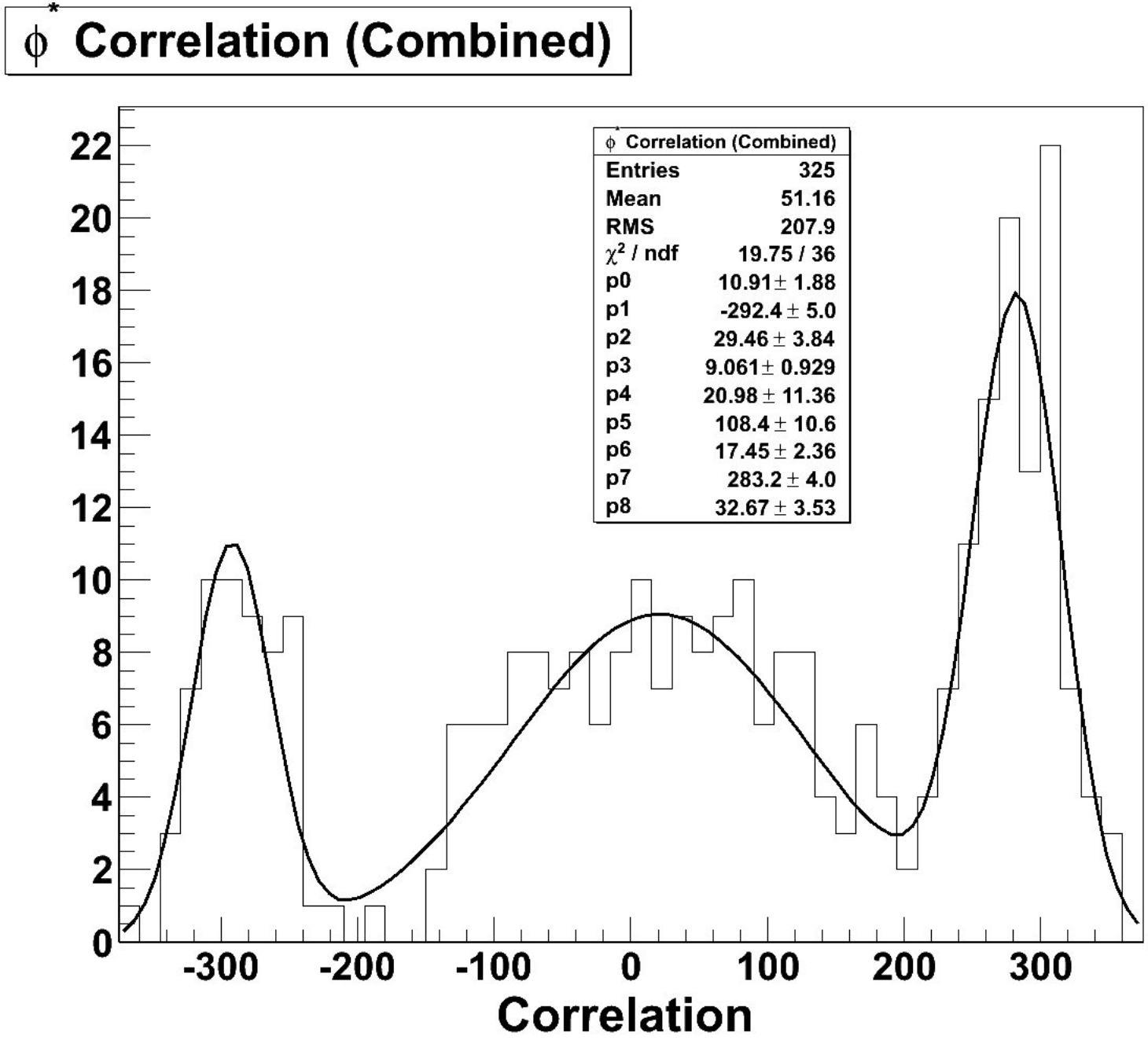

Figure 6: Combined ϕ^* Correlation

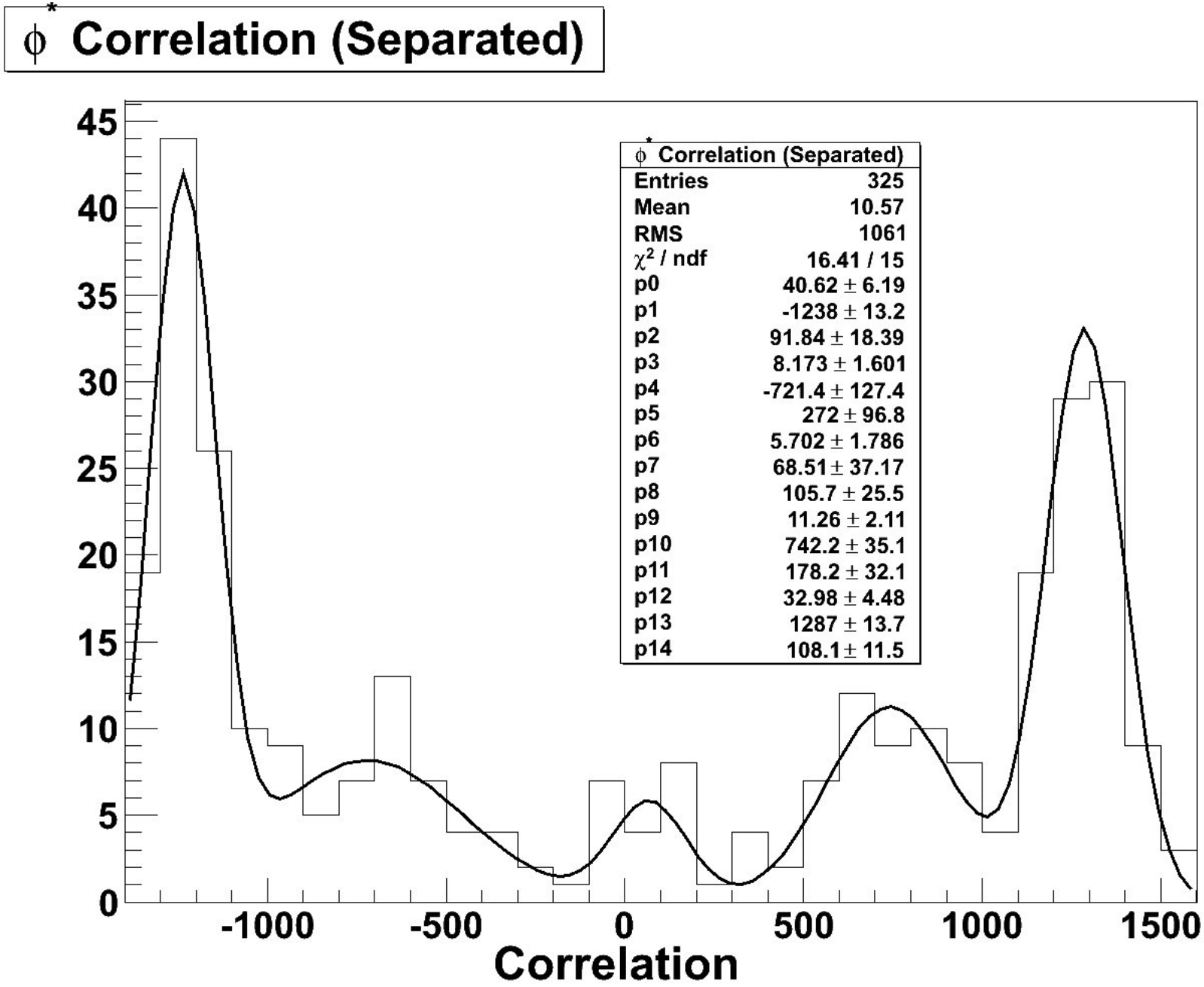

Figure 7: Separated ϕ^*Correlation

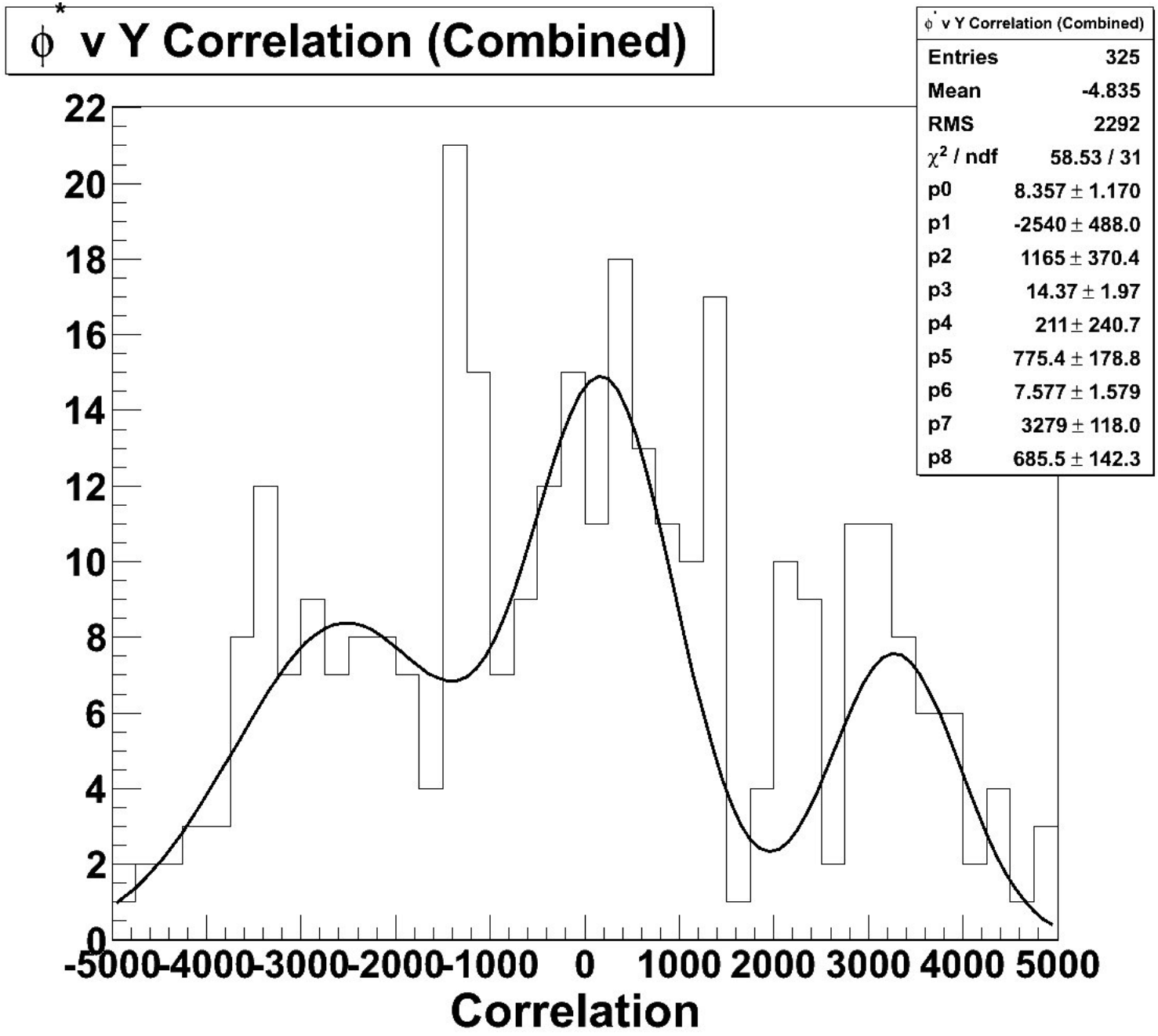

Figure 8: ϕ^* v Rapidity Correlation